Journal of Materials Processing Technology 209 (2009) 6048–6056

Contents lists available at ScienceDirect

Journal of Materials Processing Technology

journal homepage: www.elsevier.com/locate/jmatprotec

Movement patterns of ellipsoidal particle in abrasive flow machining

Liang Fang*, Jia Zhao, Bo Li, Kun Sun

The State Key Laboratory for Mechanical Behavior of Materials, Xian Jiaotong University, 28 West Xianning Road, Xian 710049, PR China

ARTICLE INFO

Keywords:
Abrasive flow machining
Particle movement pattern
Statistical calculation

ABSTRACT

Abrasive particle movement pattern is an important factor in estimating the wear rate of materials, especially, as it is closely related to the burring, buffing and polishing efficiency of the abrasive flow machining (AFM) process. There are generally two kinds of particle movement patterns in the AFM process, i.e. sliding–rubbing and rolling. In mechanism, AFM particle–workpiece interaction is taking place in any one or a combination of the possible modes: elastic/plastic deformation by grooving particle movement; elastic/plastic deformation by rolling particle movement; chip formation (micro-cutting) by grooving particle movement, ridge formation by grooving and rolling particle movement, and low-cycle fatigue wear. Grooving particle movement pattern has a greater contribution to wear mass loss of workpiece than rolling mode. Considering the machining efficiency of a machine part is predominantly dependent upon its wear mass loss speed, it can be concluded that particle movement patterns are key parameters to machining efficiency in AFM. In this paper, ellipsoidal particles are investigated to understand particle movement patterns. An analytical model of ellipsoidal geometry to determine particle movement patterns in AFM is proposed with given particle ellipticity, normal load, particle size and material hardness. From the analytical model and particle movement pattern criterion proposed by the present authors, a statistic prediction of particle movement patterns is completed by computer programmed by C++ language. It is found that a seat position of ellipsoid is an easy grooving position for a particle and a large ellipticity value predominantly increases grooving particle numbers. Smaller workpiece hardness, larger particle radius and higher normal load promote grooving of the particles. Sharper particles are much more easy to groove; moreover, grooving pattern will be predominant if particle ellipticity is below 0.8. Increasing workpiece hardness tends to decrease grooving regime while other parameters are fixed in AFM process. In three-body abrasion, hard material paired with soft material will result in more rolling particles. Abrasive contour and material hardness in many variables are two predominant parameters to give distinct influence on particle movement pattern.

1. Introduction

Abrasive flow machining (AFM) is an unconventional machining process. It can be used to produce difficult-to-reach surfaces of workpieces. It is quite suitable to produce curved smooth surfaces by burring, buffing and polishing procedure. Concerned with theoretical research in AFM process, there have been some reports (Haan and Steif, 1998; Williams and Rajurkar, 1992; Davies and Fletcher, 1995). More meaningful researches have also been done by several scientists (Gorana et al., 2006; Jain and Jain, 1999, 2004; Gorana et al., 2004; Jain et al., 1999a,b). After careful observation of AFM process, it is, then, noticed that abrasive particles in suspended flowing medium have rolling tendency besides sliding relative to workpiece surface. It is quite similar to a three-body abrasion process with strong particles sliding tendency.

Williams and Rajurkar (1992) carried out AFM experiments and concluded that material removal improves with pressure and viscosity. Experimental results from Jain and Jain (1999) show that material removal is governed by initial surface finish and workpiece hardness. Based on two-body wear, Jain (1999) proposes his mathematical model which includes the operation condition parameters to explain wear in AFM. However, theoretical results cannot match experimental data very well in surface roughness variation. It can be found that the assumptions are somewhat simple because abrasive particles are assumed to be sphere and wear process is assumed to be cutting without plastic deformation. In the same year, Jain (1999) uses neural network approach to investigate AFM, the approach has a progress in material removal prediction in AFM, but it is only a learning model to predict material removal from limited experimental data. It is the first time to predict force from rheological medium in AFM when

* Corresponding author. Tel.: +86 29 82665479; fax: +86 29 82665479.
E-mail address: fangl@xjtu.edu.cn (L. Fang).

0924-0136/$ – see front matter © 2009 Elsevier B.V. All rights reserved.
doi:10.1016/j.jmatprotec.2009.08.013

Gorana et al. (2006) develop a two-body abrasive mathematic model to predict radial and axial force on a single abrasive particle. In the model, plastic deformation is included. Unfortunately, the predicted force does not vary with the piston pressure. It has been shown that material removal increases with the piston pressure and is highly dependent on the force acted on abrasive particles.

Haan and Steif (1998) propose a model for predicting abrasive wear due to slow flows of concentrated suspensions from rheological viewpoints, which was presented for AFM wear mechanisms. Wear efficiencies are calculated and distributed in the range of 10^{-5} to 10^{-3}, which is quantitatively similar to those measured elsewhere for three-body wear by sheer coincidence. For AFM, abrasive particles are carried by semi-solid medium with pressure. The particles are constrained by the medium, but not completely. They form their own movement patterns. This feature makes AFM similar to the three-body wear to some extent.

Three-body abrasion describes a wear process where wear particles are not fixed and in loose conditions during working. Therefore, two-body abrasion is considered as a special case of three-body abrasion (Zhang et al., 2000). Two-body abrasion, then, develops if the relative positions of particles are fixed. The present authors have reported some research results on three-body abrasion from the angle of movement patterns of abrasive particles (Fang et al., 1991, 1992, 1993, 1998; Fang and Zhou, 1995). It has been concluded from those researches that the movement patterns for abrasive particles can be exactly defined as sliding and rolling.

In three-body abrasion, the morphology of worn surface becomes more complicated than that in two-body abrasion. The worn surface sometimes shows a lot of repeated plastic deformation characteristic (Fang et al., 1992, 1998; Fang et al., 1993; Fang and Zhou, 1995). That kind of surface characteristic is definitely not caused by grooving particles. When wear parameters are changed to some values range the worn surface can also show the grooving morphology, which, of course, is not caused by rolling particles (Fang et al., 1992; Fang and Zhou, 1995). The movement patterns of abrasive particles, therefore, determine the morphology of worn surface, which reflects the change of wear mechanism.

Most theoretical models for abrasive wear of a plastic material assume a single, non-rotating two-dimensional indenter (Ronen and Malkin, 1981). There are very few models for three-body abrasion, in which the particles are free to roll within the contact region, probably because of the complexity of the process. Misra and Finnie (1981) introduced a further subdivision into 'open' and 'closed' abrasion. Open three-body wear occurs when loose abrasive particles are in contact with one surface, for example, in the flow of particles in chutes and hoppers. Closed three-body wear occurs when loose abrasive particles are trapped between two sliding surfaces. In AFM process, the particles are only in contact with one surface, but not trapped, because other "surfaces" are rheological media and abrasive particles themselves. In most models for three-body abrasive wear, the particle is assumed round or spherical. In reality, abrasive particles are always in complicated geometry. Stachowiak and Stachowiak (2001) use spike parameter quadratic fit (SPQ) to characterize three-body abrasion. It is, however, difficult to predict particle movement using that parameter at present.

In the present paper, an ellipsoidal particle is assumed as the first approximation to simulate various real particle contours. Of course, that approximation is very simple, but it can characterize the particle movement pattern in AFM or three-body abrasion. To predict the movement patterns of particles, normal load, particle size, material hardness and particle ellipticity are investigated in this investigation.

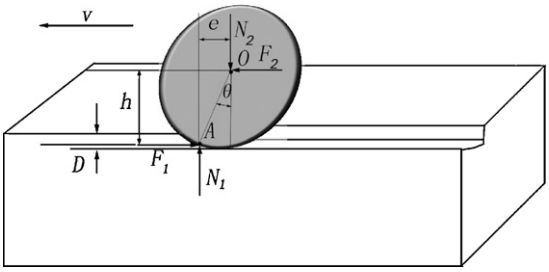

Fig. 1. Schematic of forces on an ellipsoidal abrasive particle in AFM.

2. Equivalent circle approach in evaluating the movement of ellipsoidal particles

2.1. Modeling sphere particle to evaluate movement pattern

Fig. 1 shows the sum of forces acted on a moving ellipsoidal particle. Point A is assumed as a central contact point of distributed forces on the particle by a surface, and point O, the centroid of the ellipsoidal particle. The normal load acting on the particle is N_1 and the friction force exerted by the surface is F_1, by the surface, separately. F_2 is the horizontal drive force and N_2 is the normal force exerted by the medium or other particles. v is particle movement direction, and D indentation depth. For simplicity, N_2 and F_2 are also assumed acting on the centroid of the ellipsoidal particle although the point has some variations. The difference is quite small in AFM. From the previous work by the present authors there exists also equilibrium by the relations

$$F = F_1 = F_2 \tag{1}$$

and

$$N = N_1 = N_2 \tag{2}$$

Here a driving torque moment $F{\cdot}h$ and a resistant torque $N{\cdot}e$ are defined. When $F{\cdot}h$ is less than $N{\cdot}e$, that is,

$$F \cdot h < N \cdot e \tag{3}$$

the particle will groove the surface, and on the contrary, that is true for rolling particle. From the definition of friction coefficient, that is, $\mu = F/N$, above expression (3) becomes

$$\mu_s \le \frac{e}{h} \tag{4}$$

where μ_s is the particle grooving friction coefficient. For rolling particle the following is obtained

$$\mu_r \ge \frac{e}{h} \tag{5}$$

where μ_r is the particle rolling friction coefficient.

From the previous work by the present authors, a criterion applied to predict the movement pattern of particles is

$$\frac{e}{h} \ge \mu_s = \mu_k \quad \text{(for grooving particle)} \tag{6}$$

$$\frac{e}{h} < \mu_r < \mu_k \,\text{(for rolling particle)} \tag{7}$$

For a spherical particle where there is

$$e = \frac{4}{3\pi}(r_1 + r_2) \tag{8}$$

$$h = \frac{2}{3}\left(\frac{r_1 \sin^3\alpha_1}{\alpha_1 - \sin\alpha_1\cos\alpha_1} + \frac{r_2 \sin^3\alpha_2}{\alpha_2 - \sin\alpha_2\cos\alpha_2}\right) \tag{9}$$

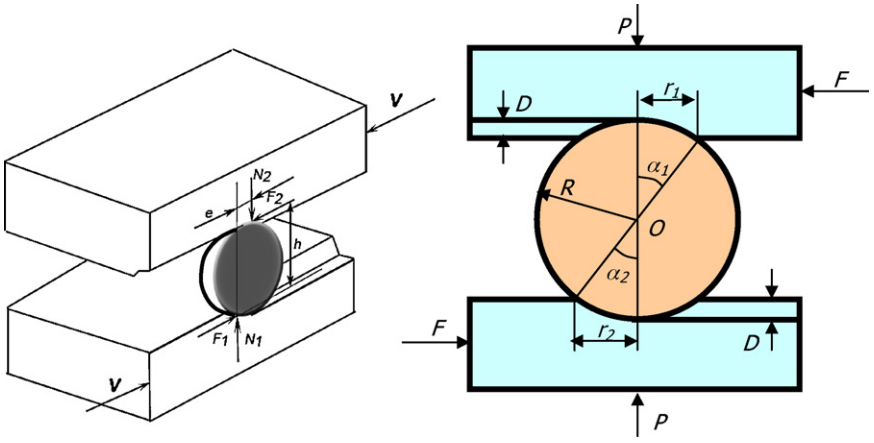

Fig. 2. Schematic illustration of force analysis on an abrasive particle.

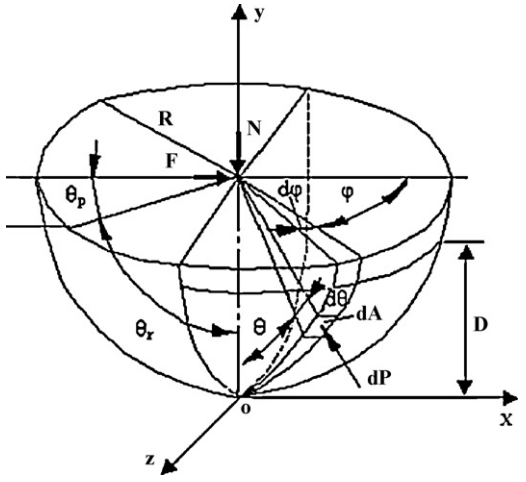

Fig. 3. Geometric parameters of a half sphere used for calculating μ_k.

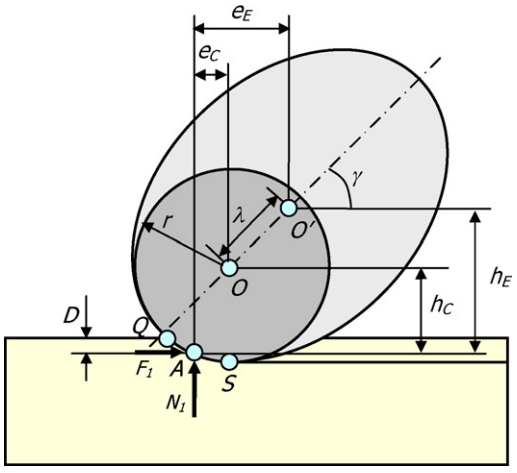

Fig. 4. Parameters of ellipsoidal abrasive particle cross-section using a spherical approximation method.

$$\frac{e}{h} = \frac{2P}{\pi^2 R^2 H_1} \cdot \frac{\xi_1^{1/2} + \xi_2^{1/2}}{\xi_1^{3/2} + (H_2/H_1)\xi_2^{3/2}}, \quad \xi_1 = \left[1 - \left(1 - \frac{P}{\pi R^2 H_1}\right)^2\right],$$
$$\xi_2 = \left[1 - \left(1 - \frac{P}{\pi R^2 H_2}\right)^2\right] \tag{10}$$

$$\mu_k = \frac{F}{N} = \frac{(2\theta_r - \sin 2\theta_r) + 4\mu \int_0^{\theta_r}\int_0^{\pi/2} (\sin\theta(\cos^2\varphi\cos^2\theta + \sin^2\varphi)/\sqrt{\cos^2\varphi\cos^2\theta + \sin^2\varphi})\, d\theta\, d\varphi}{\pi \sin^2\theta_r - 4\mu \int_0^{\theta_r}\int_0^{\pi/2} (\cos\varphi\cos\theta\sin^2\theta/\sqrt{\cos^2\varphi\cos^2\theta + \sin^2\varphi})\, d\theta\, d\varphi} \tag{11}$$

It can be seen from Eq. (10) that e/h is controlled by normal load P, particle size R, surface hardness H_1 and H_2. Besides, it has also mentioned before that e/h is also related to geometric parameters of particle itself. The e/h is, therefore, a systematic parameter related to whole wear system. Other parameters in above equations can be found in Figs. 2 and 3.

2.2. Modeling ellipsoidal particle using equivalent circle approach to evaluate movement pattern

In real world an abrasive particle always behaves irregular in geometry. However, it should have a statistical discipline. In this research an ellipsoidal particle is assumed as the first approximation. To illustrate the ellipsoidal particle movement pattern in AFM, a circle approximation approach is used at first to get indentation and contact point position as shown in Fig. 4. For simplicity, an equivalent circle approach is used in which two-dimensional analysis is applied. A circle and an ellipsoid are overlapped together to make the circle particle boundary coincident with the ellipsoid at the geometric lowest point S and the contact point of the circle Q with surface also coincident with that of the ellipsoid as shown in Fig. 4. In Fig. 4, a separated angle is defined as rotation angle of ellipsoid γ between the center of a circle point O and the center of ellipsoid O'. A becomes a working point of resultant force N_1 and F_1 for the circle. r is the radius of the circle and λ is the center distance of the circle and ellipsoid. Thus, the resultant forces, i.e. N_1 and F_1 of the circle can be approximately considered equal to that of the ellipsoid.

Because e/h value for the equivalent circle can be easily got from expressions (8)–(10), the e/h for the ellipsoid can be directly got by following equations

$$\begin{cases} e_E = e_C + \lambda\cos\gamma \\ h_E = h_C + \lambda\sin\gamma \end{cases} \tag{12}$$

where e_E is a horizontal distance of the ellipsoid centroid, e_C a horizontal distance of the circle centroid, h_E a vertical distance of the ellipsoid centroid and h_C is a vertical distance of the circle centroid.

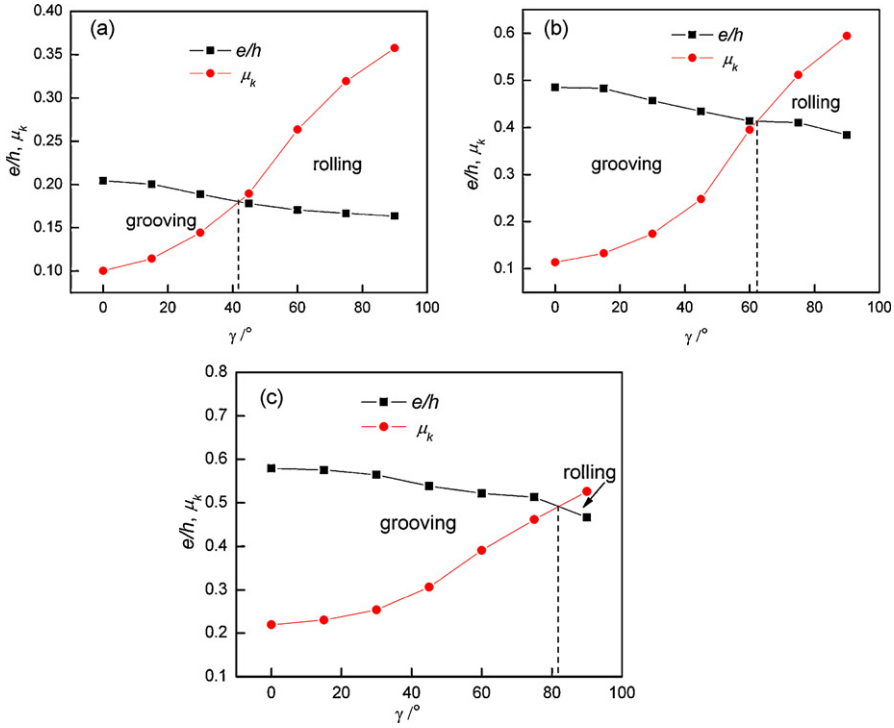

Fig. 5. Relationship between e/h and μ_k with varying rotation angle γ in different normal load. (a) $P = 0.1$ N, (b) $P = 0.5$ N, and (c) $P = 0.7$ N.

In order to predict the movement patterns of the ellipsoidal particle in a given condition, a program using VC++ language platform is compiled. Materials used in the prediction are AISI 1080 steel (294 MPa BNH), AISI 1045 steel (182 MPa BNH), AISI 1020 steel (111 MPa BNH) and pure copper (72 MPa BNH), separately. Long semi axis a of ellipsoid is chosen as 0.10, 0.11, 0.12, 0.13, 0.14 and 0.15 mm individually. The normal load P was 0.1, 0.2, 0.3, 0.4, 0.5, 0.7 N individually. Ellipticity b/a is 0.6, 0.7, 0.8, 0.9 and 1.0 individually. Rotation angle γ was 0°, 15°, 30°, 45°, 60°, 75° and 90° individually. The adhere coefficient μ between the particle and surface must be got at first when calculating μ_k by expression (11). Gaussian integration method is used to solve integrals in expression (11) to get μ_k. Hisakado et al. (1987) used pyramid indenter of diamond to scratch steel and copper. In his calculation of adhere coefficient $\mu = 0.12$ which can be substituted into his friction coefficient μ_k expression. The theoretical data matches experimental values quite well in his work, therefore, the present authors also borrow the value $\mu = 0.12$ in the present calculations.

2.3. Movement prediction of two-dimensional ellipsoidal particle relative to rotation angle

Fig. 5 shows the curves of e/h and μ_k of ellipsoidal particle for pure copper with $a = 0.15$ mm, and $b/a = 0.8$. It is shown from Fig. 5 that the intersection point of e/h and μ_k move towards to large angle γ value with increasing normal load P. In expression (6) and (7) of particle movement criterion, the part of data e/h becomes regime of particle grooving. By comparing the three curves in Fig. 5 particle grooving probability increases with increasing normal load P. When parameters are defined by $P = 0.5$ N, $a = 0.15$ mm, and $b/a = 0.8$ with changing material hardness, the particle grooving probability tends to decrease with increasing materials hardness with the similar principle as shown in Fig. 6.

It can be concluded from Figs. 5 and 6 that e/h always keeps the largest at $\gamma = 0°$, where μ_k keeps the minimum, vice versa. It means abrasive particles have their largest grooving tendency in their seating position. Because of the principle of energy minimum, it is believed that every particle tends to be rotated to its seat position before it grooves surface steadily. Therefore, in the following sections the movement pattern model of oblate sphere is proposed and discussed in the seat position. The movement pattern prediction of oblate sphere using seating position belongs to a conservative estimation for grooving particle.

3. Oblate sphere approach in evaluating the movement of ellipsoidal particles

3.1. Modeling oblate sphere particle to evaluate movement pattern

Ishizuka (1977)'s μ_k model is only capable to be used in ideal sphere geometry. In order to be applied to an oblate sphere particle, a mapping transformation technique for oblate sphere space is utilized. In that technique, the short semi-axis of oblate sphere is multiplied a coefficient and let it equal to the long semi axis. Finally, an oblate sphere in Cartesian coordinate is transformed to ideal sphere system and Ishizuka's μ_k model can be reasonably used. The detailed process can be provided in Appendix A. μ_k of oblate sphere particle in seat position is shown in Eq. (13).

$$\mu_k = \frac{F}{N} = \frac{(2\theta_r - \sin 2\theta_r) + 4\mu \int_0^{\theta_r}\int_0^{\pi/2}(b/a\sin\theta(\cos^2\varphi\cos^2\theta + (\cos^2\theta\sin^2\varphi/1 - (b^2/a^2)\sin^2\theta))/\sqrt{\cos^2\varphi\cos^2\theta + (\cos^2\theta\sin^2\varphi/1 - (b^2/a^2)\sin^2\theta)}d\theta d\varphi}{\pi\sin^2\theta_r - 4\mu\int_0^{\theta_r}\int_0^{\pi/2}(\cos\varphi\cos\theta(b^2/a^2)\sin^2\theta/\sqrt{\cos^2\varphi\cos^2\theta + (\cos^2\theta\sin^2\varphi/1 - (b^2/a^2)\sin^2\theta)}d\theta d\varphi} \quad (13)$$

3.2. Movement prediction of oblate sphere particle in AFM

Different parameters, such as, normal load, particle size and hardness are used in the prediction to investigate response of par-

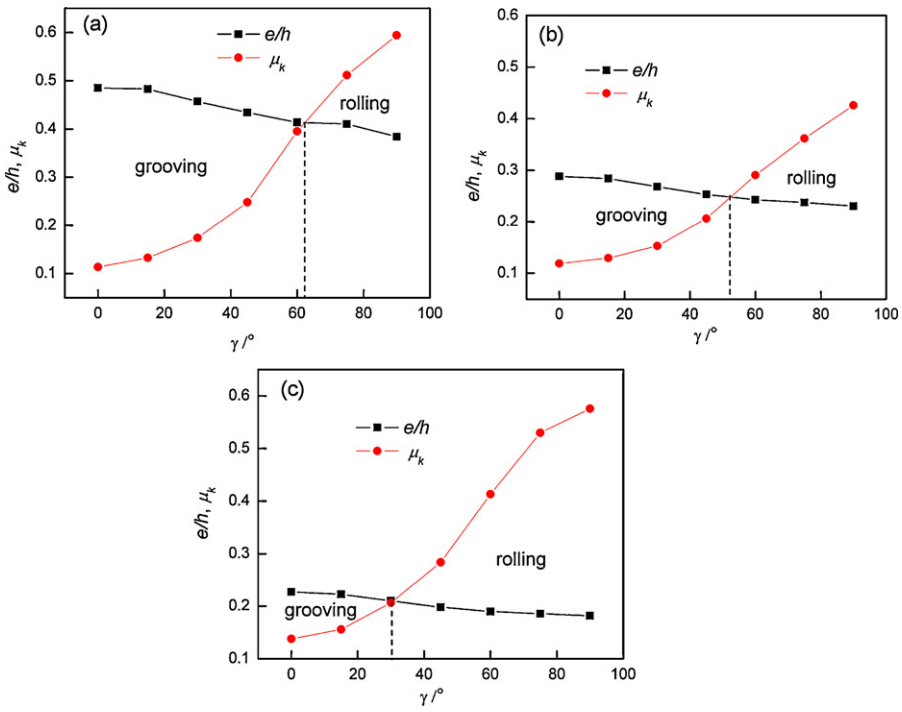

Fig. 6. Relationship between e/h and μ_k with varying rotation angle γ with different hardness in AFM process. (a) Pure copper, (b) AISI 1045 steel, and (c) AISI 1080 steel.

ticle movement patterns. Three-dimensional surface figures are drawn to explain particle movement tendency with varying parameters, such as, normal load P and semi-major axis a. Fig. 7 shows the influence of normal load P and long semi-axis length a on e/h and μ_k in seat position of oblate sphere particles for AISI 1045 steel. It is explained from Fig. 7 that both e/h and μ_k increase with normal load P. The larger the semi-major axis length a, the smaller the e/h and μ_k. It is concluded that grooving regime is reduced with

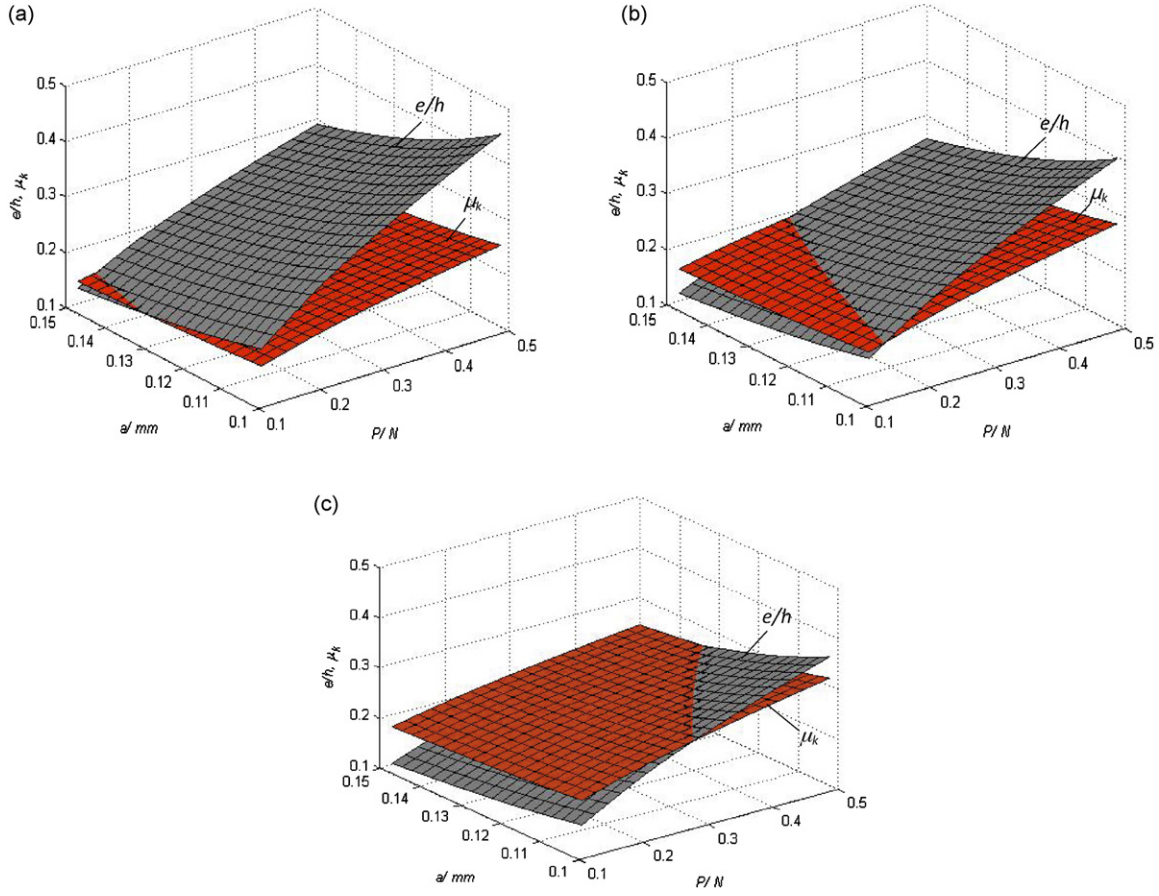

Fig. 7. Relationships of e/h, μ_k to normal load P and semi-major axis length a with different ellipticities in AFM process (e/h in grey color and μ_k in red color) (a) $b/a = 0.8$, (b) $b/a = 0.9$, and (c) $b/a = 1.0$. (For interpretation of the references to color in this figure legend, the reader is referred to the web version of the article.)

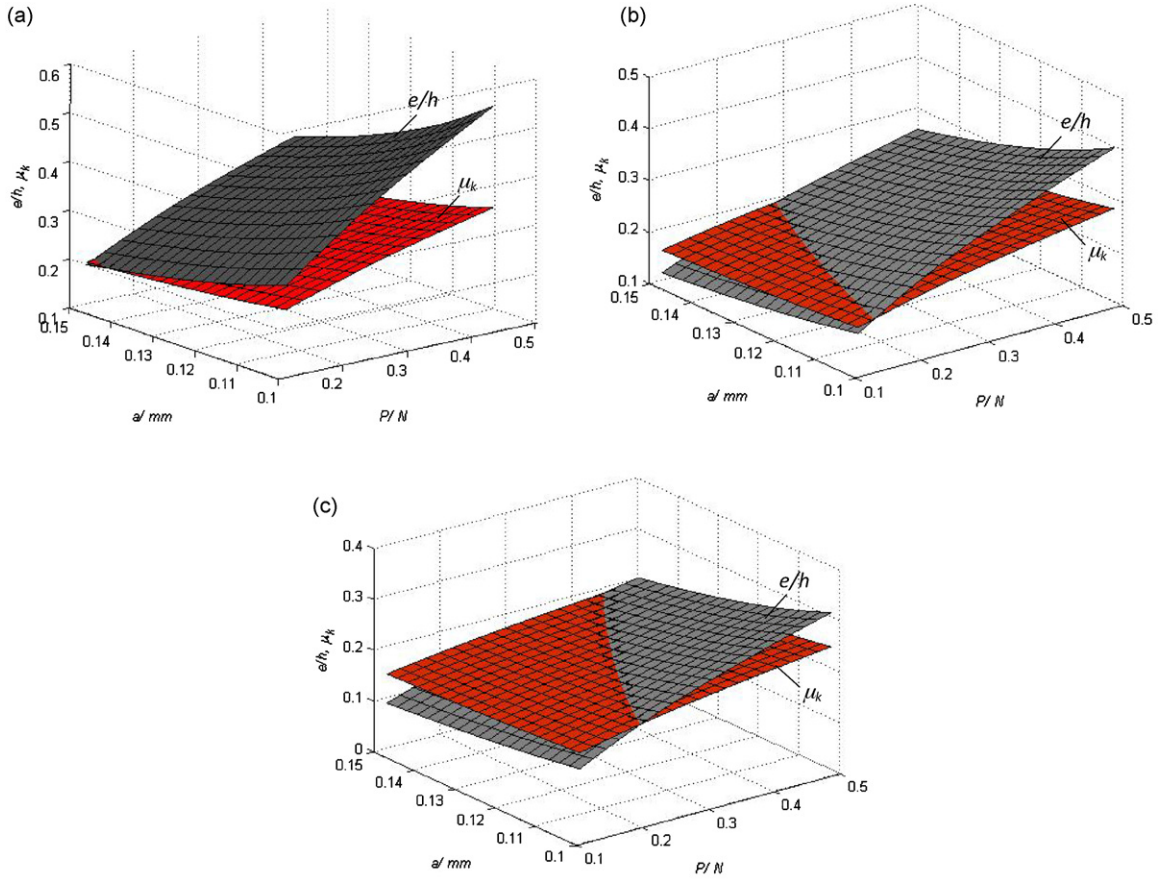

Fig. 8. Relationships of e/h, μ_k to normal load P and semi-major axis length a for different materials in AFM process (e/h in grey color and μ_k in red color) (a) pure copper, (b) AISI 1045 steel, and (c) AISI 1080 steel. (For interpretation of the references to color in this figure legend, the reader is referred to the web version of the article.)

b/a increasing to one if three figures in Fig. 7 are compared. When $b/a = 0.8$, the particles with a smaller normal loads and larger sizes tend to rolling in Fig. 7(a) and the particles with a larger normal loads and smaller sizes tend to grooving when $b/a = 1.0$ in Fig. 7(c).

Fig. 8 shows the influence of normal load P and semi-major axis length a on e/h and μ_k when $b/a = 0.9$ in the seat position of oblate sphere particles. It is shown from Fig. 8 that grooving regime decreases with increasing material hardness. The particles tend to rolling at smaller loads and larger sizes for soft materials, such as, pure copper. While the particles grooves at larger loads and smaller sizes for hard materials like AISI 1080 steel as shown in Fig. 8(a) and (c).

4. Evaluation of the movement of ellipsoidal particles in three-body abrasion

Above approach can be easily extended to particle movement pattern evaluation in three-body abrasion process. In three-body abrasion particles are embedded between two relative moving surfaces and contacted with both surfaces. The previous e/h value for AFM is different for three-body abrasion. The difference is that there are two matched surfaces in three-body abrasion, compared to AFM process. Hence, the movement patterns of ellipsoidal particles are also necessary to be evaluated for two matched surfaces with different hardness.

Fig. 9 shows the influence of normal load P and semi-major axis length a on e/h and μ_k in seat position of ellipsoidal particles for three material pairs with different hardness. With increasing material hardness of one surface, particle grooving regime decreases as a whole. Comparing the three figures in Fig. 9, larger particle sizes are beneficial to increase the regime of grooving than smaller particles.

5. Discussion

From Figs. 5–8, it can be seen that particle movement pattern of AFM is influenced by parameters, such as, material hardness, normal load, particle size, ellipticity, etc. By careful comparison of the data, decreasing material hardness and increasing normal load result in grooving regime. It has been shown from AFM tests by Jain et al. (1999a,b) that greater extrusion pressure and lower workpiece hardness increase the machining efficiency. The result matches our prediction very well. The ellipticity of the particles can be approximately borrowed as a parameter of roundness. It is thought to be reasonable that much sharper particles use smaller ellipticity values. In AFM process, particles are used as a cutting tool. As machining time increases, sharp particles always become blunt so that it causes work efficiency deteriorated. As our calculations as shown in Fig. 7, ellipticity is a predominant monitor to give a strong influence on particle movement patterns. With increasing b/a varied from 0.8 to 1.0, almost all particles which are in grooving regime in $b/a = 0.8$ are changed to rolling regime in $b/a = 1.0$.

The influence of particle size on movement patterns is also clear. In our calculations, larger particle sizes are generally beneficial to enlarge the regime of grooving as indicated in Figs. 7–9. That result should be consistent with AFM experimental data. In AFM process, the larger the particle sizes, the more the work efficiency When particle sizes in medium are increased it always improves the work efficiency although the roughness of workpiece is not satisfied. Therefore, a medium with fine particles is often replaced in this case to smooth the surface of workpiece. As for viscosity of medium, an AFM process with a larger medium viscosity will definitely increase the extrusion pressure, which makes particles locate in grooving regime. Finally, the cutting efficiency of AFM is improved.

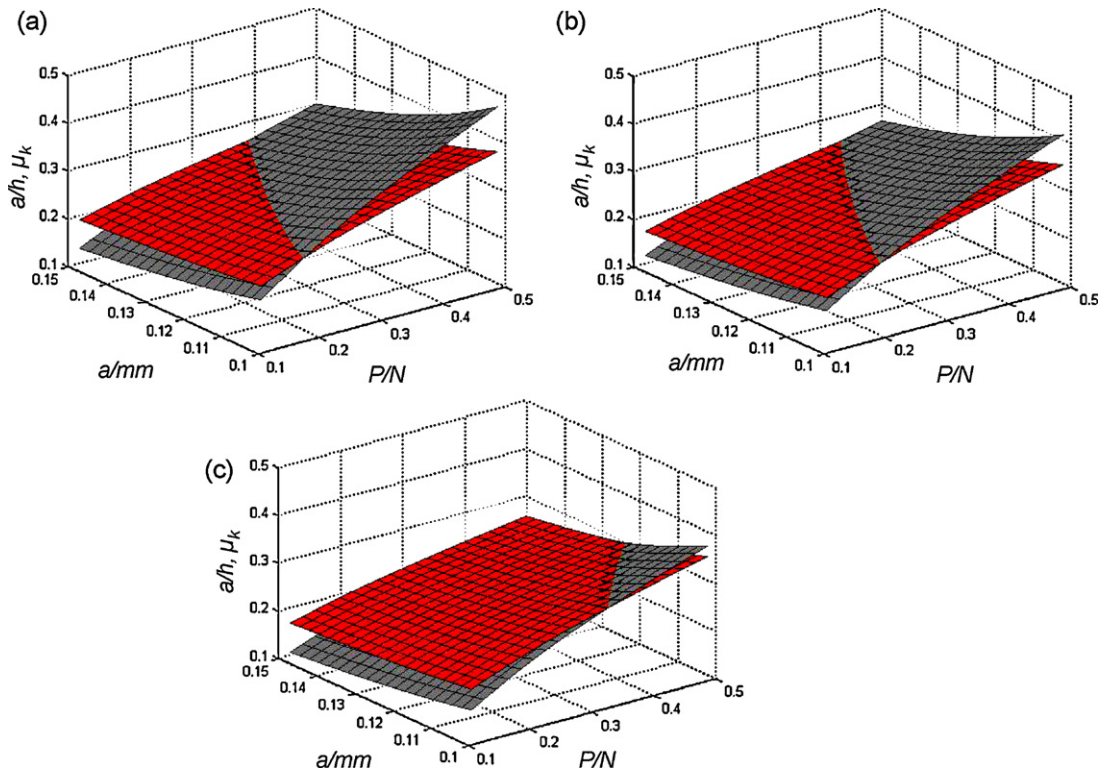

Fig. 9. Relationships of e/h, μ_k to normal load P and semi-major axis length a for different material pairs when $b/a = 1.0$ in three-body abrasion (grey – e/h, red – μ_k) (a) A36-A36, (b) A36-AISI 1045, and (c) A36-AISI 1080. (For interpretation of the references to color in this figure legend, the reader is referred to the web version of the article.)

In three-body abrasive wear, hard material paired with soft material will result in more rolling particles as shown in Fig. 9. It is therefore imaged that the total wear loss may be decreased in this case, compared to the material pairs of A36/A36 and A36/AISI 1045, respectively.

6. Conclusions

(1) A criterion for ellipsoidal particle movement patterns is proposed in abrasive flow machining process. Parameters such as workpiece hardness, particle size, normal load, and ellipticity are directly related to wear and finally control particle movement patterns.
(2) Ellipsoidal particles behave grooving and rolling in abrasive flow machining process. Smaller workpiece hardness, larger particle radius and higher normal load promote grooving of the particles. Sharper particles are much more easy to groove; moreover, grooving pattern will be predominant if particle ellipticity is below 0.8.
(3) Increasing workpiece hardness results in decreasing grooving regime while other parameters are fixed in AFM process. In three-body abrasion hard material paired with soft material will result in more rolling particles.
(4) The present prediction using the particle movement criterion is in good agreement with AFM experiments.

Nomenclature

a	semi-major axis length of ellipsoidal particle (mm)
b	semi-minor axis length of ellipsoidal particle (mm)
b/a	ellipticity of ellipsoidal particle
D	particle indentation depth (mm)
e	horizontal distance between normal loads (mm)
e_c	a horizontal distance of the approximated circle centroid (mm)
e_e	a horizontal distance of the ellipsoid centroid (mm)
F	friction force (N)
F_1	friction force acted on particle by workpiece surface (N)
F_2	friction force acted on particle by suspended medium (N)
h	normal distance between friction forces (mm)
h_c	a vertical distance of the approximated circle centroid (mm)
h_e	a vertical distance of the ellipsoid centroid (mm)
H	Brinell hardness (MPa)
H_1	surface 1 hardness (MPa)
H_2	surface 2 hardness (MPa)
N	normal load (N)
N_1	normal load acted on particle by workpiece surface (N)
N_2	normal load acted on particle by suspended medium (N)
P	normal load on spherical particle (N)
R	particle radius (mm)
r_1	half the width of indentation for surface 1 (mm)
r_2	half the width of indentation for surface 2 (mm)
r	radius of the approximated circle (mm)
μ	friction coefficient
μ_s	particle grooving friction coefficient
μ_r	particle rolling friction coefficient
α_1	contact angle related to surface 1 (°)
α_2	contact angle related to surface 2 (°)
ξ_1	parameter related to surface 1
ξ_2	parameter related to surface 2
μ_k	friction coefficient causing material yield during particle grooving
θ	angle of unit plane to y axis for a semi-sphere surface (°)
φ	angle of unit plane to x axis for a semi-sphere surface (°)

θ_r angle of point coordinate of equator to y axis for semi-sphere (°)
λ center distance of the circle and ellipsoid (mm)
γ rotation angle of the ellipsoidal particle (°)

Acknowledgement

This work was supported by the National Natural Science Foundation of China Grant 50475089: Abrasive Flow Machining Investigated by Low-Cycle Fatigue and Monte Carlo Method.

Appendix A. Derivation of μ_k model in ellipsoidal coordinate system

In sphere coordinate system there is:

$$\begin{cases} x = r\cos\theta\cos\varphi, & (-\pi/2 \le \theta \le \pi/2) \\ y = r\cos\theta\sin\varphi, & (0 \le \varphi < 2\pi) \\ z = r\sin\theta. \end{cases} \tag{A1}$$

and in rotating ellipsoid coordinate system there is:

$$\begin{cases} x = a\cos\theta\cos\varphi, & (-\pi/2 \le \theta \le \pi/2) \\ y = a\cos\theta\sin\varphi, & (0 \le \varphi < 2\pi) \\ z = b\sin\theta. \end{cases} \tag{A2}$$

Assume

$$z' = \frac{a}{b}\cdot z = a\cdot\sin\theta \tag{A3}$$

A sphere coordinate system (A4) contains x, y, z' was obtained by combining (A2) and (A3),

$$\begin{cases} x = a\cos\theta\cos\varphi, & (-\pi/2 \le \theta \le \pi/2) \\ y = a\cos\theta\sin\varphi, & (0 \le \varphi < 2\pi) \\ z' = a\sin\theta. \end{cases} \tag{A4}$$

Cartesian coordinate system expression of μ_k was obtained as:

$$\mu_k = \frac{F}{N} = \frac{(2\theta_r - \sin 2\theta_r) + 4\mu\int_0^{\theta_r}\int_0^{\pi/2}(z/r\cdot(x^2/r^2 + y^2/(r^2 - z^2))/\sqrt{x^2/r^2 + y^2/(r^2 - z^2)})\,d\theta\,d\varphi}{\pi\sin^2\theta_r - 4\mu\int_0^{\theta_r}\int_0^{\pi/2}((x/r)\cdot(z^2/r^2)/\sqrt{x^2/r^2 + y^2/(r^2 - z^2)})\,d\theta\,d\varphi} \tag{A5}$$

Combine (A3), (A4) and (A5), ellipsoidal particle μ_k expression in ellipsoid system was obtained:

$$\mu_k = \frac{F}{N} = \frac{\begin{array}{c}(2\theta_r - \sin 2\theta_r) + 4\mu\int_0^{\theta_r}\int_0^{\pi/2}(b/a\sin\theta(\cos^2\varphi\cos^2\theta + (\cos^2\theta\sin^2\varphi/1 \\ -(b^2/a^2)\sin^2\theta))/\sqrt{\cos^2\varphi\cos^2\theta + (\cos^2\theta\sin^2\varphi/1 - (b^2/a^2)\sin^2\theta))}\,d\theta\,d\varphi\end{array}}{\pi\sin^2\theta_r - 4\mu\int_0^{\theta_r}\int_0^{\pi/2}(\cos\varphi\cos\theta(b^2/a^2)\sin^2\theta/\sqrt{\cos^2\varphi\cos^2\theta + ((\cos^2\theta\sin^2\varphi)/(1 - (b^2/a^2)\sin^2\theta))})\,d\theta\,d\varphi} \tag{A6}$$

Appendix B. Expressions of key points coordinates of an ellipsoidal particle using sphere approximation

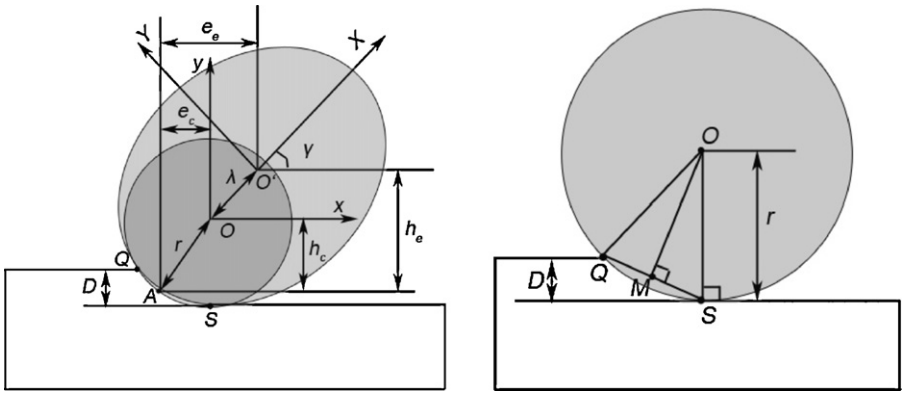

Above two figures showed the geometric parameters in the sphere approximation. In the two figures, two coordinate systems x–y and X–Y are created for numerical calculation. Here are expressions for key points. Point coordinates in x–y coordinate system:

$$A : (-e_c, -h_c);\ e_1 = \frac{4}{3\pi}(r_1 + r_2);$$
$$h_1 = \frac{2}{3}\left(\frac{r_1\sin^3\alpha_1}{\alpha_1 - \sin\alpha_1\cos\alpha_1} + \frac{r_2\sin^3\alpha_2}{\alpha_2 - \sin\alpha_2\cos\alpha_2}\right)$$
$$Q : (-\sqrt{r^2 - (r - D)^2}, -r + D);$$
$$S : (0, -r);$$

Above coordinates can be obtained in X–Y coordinate system through relationship between x–y and X–Y coordinate systems. Assume coordinates of a random point in x–y can be expressed as (x_a, y_a), and in X–Y (X_a, Y_a), there can be relationship:

$$\begin{cases} X_a = \lambda\cdot\cos\gamma + x_a\cdot\cos\gamma + y_a\cdot\sin\gamma \\ Y_a = \lambda\cdot\sin\gamma + x_a\cdot\sin\gamma - y_a\cdot\cos\gamma \end{cases}$$

Expression of r:

$$r = \frac{L}{\sin(2\cdot arctg\, D/L)}$$

Appendix C. Expressions of e/h of a sphere particle model

In Fig. 2, the radius of a sphere particle is R, the hardness of surface 1 H_1, the hardness of surface 2, H_2 and normal load P. The elastic deformation relative to plastic deformation is quite less and can be ignored. The relation of indented depth of particle D to surface hardness can be expressed as

$$D = \frac{P}{\pi RH} \tag{C1}$$

It is considered that load acted on the contact area is equally distributed. Considering actual contact surface geometry, it is given

$$e = \frac{4}{3\pi}(r_1 + r_2) \tag{C2}$$

where r_1, r_2 is the half the width of indentation for surfaces 1 and 2, separately as shown in Fig. 2. Thus

$$h = \frac{2}{3}\left(\frac{r_1 \sin^3\alpha_1}{\alpha_1 - \sin\alpha_1\cos\alpha_1} + \frac{r_2 \sin^3\alpha_2}{\alpha_2 - \sin\alpha_2\cos\alpha_2}\right) \tag{C3}$$

where α_1, α_2 is the contact angle related to surfaces 1 and 2, separately. Because $D \ll R$, that is, α_1 and α_2 are quite small. From the expanded expression of Taylor series, there are $\alpha_1 \approx r_1/R$ and $\alpha_2 \approx r_2/R$. Substituting into expression (C3), the following is obtained

$$h = \frac{2}{3R}\left(\frac{r_1^3}{D_1} + \frac{r_2^3}{D_2}\right) \tag{C4}$$

Finally, substituting Eq. (C1) into Eqs. (C2) and (C4) separately, the following is obtained

$$\frac{e}{h} = \frac{2P}{\pi^2 R^2 H_1} \cdot \frac{\xi_1^{1/2} + \xi_2^{1/2}}{\xi_1^{3/2} + \frac{H_2}{H_1}\xi_2^{3/2}} \tag{C5}$$

where

$$\xi_1 = \left[1 - \left(1 - \frac{P}{\pi R^2 H_1}\right)^2\right] \tag{C6}$$

$$\xi_2 = \left[1 - \left(1 - \frac{P}{\pi R^2 H_2}\right)^2\right] \tag{C7}$$

It can be seen from Eq. (C5) that e/h is controlled by normal load P, particle size R, surface hardness H_1 and H_2. Besides, it has also mentioned before that e/h is also related to geometric parameters of particle itself. The e/h is, therefore, a systematic parameter related to whole wear system.

References

Davies, P.J., Fletcher, A.J., 1995. The assessment of the rheological characteristics of various polyborosiloxane/grit mixtures as utilized in the abrasive flow machining process. In: Proceedings of the Institution of Mechanical Engineers, vol. 209, pp. 409–418.

Fang, L., Zhou, Q.D., 1995. A statistical model describing wear traces in three-body abrasion. Tribotest 2, 47–53.

Fang, L., Zhou, Q.D., Li, Y.J., 1991. An explanation of the relation between wear and material hardness in three-body abrasion. Wear 151, 313–321.

Fang, L., Kong, X.L., Zhou, Q.D., 1992. A wear tester capable of monitoring and evaluating the movement pattern of abrasive particles in three-body abrasion. Wear 159, 115–120.

Fang, L., Kong, X.L., Su, J.Y., Zhou, Q.D., 1993. Movement patterns of abrasive particles in three-body abrasion. Wear 162–164, 782–789.

Fang, L., Zhou, Q.D., Rao, Q.C., 1998. An experimental simulation of cutting wear in three-body abrasion. Wear 218, 188–194.

Gorana, V.K., Jain, V.K., Lal, G.K., 2004. Experimental investigation into cutting forces and active grain density during abrasive flow machining. International Journal of Machine Tools & Manufacture 44, 201–211.

Gorana, V.K., Jain, V.K., Lal, G.K., 2006. Forces prediction during material deformation in abrasive flow machining. Wear 260, 128–139.

Haan, J.J., Steif, P.F., 1998. Abrasive wear due to the slow flow of a concentrated suspension. Wear 219, 177–183.

Hisakado, T., Mori, M., Kumehara, H., Suda, H., 1987. Analyses of wear rate due to micro-asperities and transferred particles on hard asperities. Wear 120, 337–351.

Ishizuka, S., 1977. Influence of ploughing and shearing on coefficient of friction (3rd Report). Lubrication, JSME 22, 669–676.

Jain, R.K., Jain, V.K., 1999. Simulation of surface generated in abrasive flow machining process. Robotics and Computer Integrated Manufacturing 15, 403–412.

Jain, R.K., Jain, V.K., 2004. Stochastic simulation of active grain density in abrasive flow machining. Journal of Materials Processing Technology 152, 17–22.

Jain, R.K., Jain, V.K., Dixit, P.M., 1999a. Modeling of material removal and surface roughness in abrasive flow machining process. International Journal of Machine Tools & Manufacture 39, 1903–1923.

Jain, R.K., Jain, V.K., Kalra, P.K., 1999b. Modelling of abrasive flow machining process: a neural network approach. Wear 231, 242–248.

Misra, A., Finnie, I., 1981. On the size effect in abrasive and erosive wear. Wear 63, 33–39.

Ronen, A., Malkin, S., 1981. Wear mechanisms of statically loaded hydrodynamic bearings by contaminant abrasive particles. Wear 68, 371–389.

Stachowiak, G.B., Stachowiak, G.W., 2001. The effects of particle characteristics on three-body abrasive wear. Wear 249, 201–207.

Williams, R.E., Rajurkar, K.P., 1992. Stochastic modeling and analysis of abrasive flow machining. Transaction of ASME, Journal of Engineering for Industry 114, 74–81.

Zhang, X.F., Fang, L., Xing, J.D., 2000. Relation between two-body abrasion and three-body abrasion. Journal of Xi'an Highway University 20 (3), 93–97.